International Journal of Smart Home
Vol.8, No.1 (2014), pp.35-44
http://dx.doi.org/10.14257/ijsh.2014.8.1.05

Picture Enhancement and Enlargement Algorithm on a Small Infrared Images

Gwanggil Jeon

Department of Embedded Systems Engineering, Incheon National University
119 Academy-ro, Yeonsu-gu, Incheon 406-772, Korea
gjeon@incheon.ac.kr

Abstract

A thermal infrared images obtained by a FLIR infrared cameras can be used to inspect the malfunction or energy strength of warmth in a location. However, generally the resolution of thermal infrared images is smaller than that of optical images, image enlargement approach is requested. In this paper, we studied on filter design algorithm for image upsampling and horizontally, vertically, or horizontally-vertically. Through the training process, the most appropriate filter coefficients are assigned to achieve a better performance. In a comparison with different sized filters and existing upsampler, it is clearly seen that bigger filter outperforms all other smaller filters in terms of both objective and visual quality.

Keywords: *thermal infrared images, image enhancement, energy strength*

1. Introduction

The thermal infrared images are one of models of infrared images. Thermographic cameras such as FLIR cameras [1, 2] discern radiation in the infrared range of the electromagnetic spectrum and create images of such radiation [3-5]. This is called thermograms. All things emit infrared radiation and the quantity of radiation sent out by an object intensifies with degree of hotness (or temperature). Therefore, warm-blooded animals such as human, dogs, birds become easily visible against the environment in daytime or night [6, 7].

One of main advantages of thermal infrared images is thermal infrared images display optical pictures of temperatures over a certain area, and we may compare the temperature on each location. Thus, thermal infrared images can be used to assess or evaluate in locations where it is unreachable or dangerous. Also, thermal infrared images can be used as a diagnostic purpose, thus it can be used as a non-destructive test method. For example, thermal infrared images can be used to search imperfection or artifacts in construction areas where pipes, shafts, metal, and plastic parts are inspected [8-10]. Moreover, thermal infrared images can be used in an area with less luminance. Figure 1 shows an example of optical picture and its low resolution thermal infrared picture.

In this paper, we propose an image upsampling algorithm for low resolution thermal infrared images. The proposed method is for enhancing a low resolution thermal infrared image captured by thermographic cameras such as FLIR cameras. The scenario we assumed is that we firstly reduce the size of the thermal infrared image captured by FLIR cameras, and reconstruct the original size of the thermal infrared image by means of designed filter.

The remainder of the article is arranged as follows. In Section 2, the proposed method is described in detail. Simulation results demonstrate the performance of the proposed method in Section 3. The paper is concluded with an overall discussion in Section 4.

ISSN: 1975-4094 IJSH

(a) (b)

Figure 1. (a) An Example of Optical Image and (b) Thermal Infrared Image of (a) Obtained by FLIR Infrared Camera

2. Thermal Infrared Image Upsampling

The signal upsampling is a process of increasing of image sampling rate. In this paper, we adopt traditional least squares [11, 12] method (LSM) in our upsampling algorithm. The LSM has two stages. One is training stage using ground truth test images where one can obtain the best filter with certain coefficient to reconstruct image. The other one is to filter the imperfect image to obtain the reconstructed images. To conduct the second stage, filters must be obtained, in other words, the first stage must be executed before the second stage. Some applications merge above two stages at the same time, however the system becomes slow and eventually causes large computational cost. Figure 2 shows the process of the proposed LSM system.

To conduct the first stage, we firstly convert ground truth image into downsampled image. The original image is used as the ground truth image which is the goal of our reconstructed image. The training stage uses ground truth image and its downsampled image as the training substances and apply LSM to obtain certain coefficients with different size. Normally the filter size is determined as odd numbers such as 3×3, 5×5, *etc*. There are many scenarios to downsample an image. For example, an image can be downsampled horizontally with the factor of N or can be downsampled vertically or diagonally with the factor of N. Also, the factor N can vary with different integer number. In this paper, we assume the parameter N as even number. Finally the best coefficients of filter are determined by having the performance metric minimized by means of statistics. In this paper, the adopted performance metric is mean squared error (MSE). We adopted traditional LSM in our system. By means of LSM, filter coefficients are determined, and we use the same filter to estimate reconstructed image. As described in the previous paragraph, the set of filter coefficients are determined in the training stage using original and the downsampled images. The determined coefficients are chosen in accord with a k^{th} order model, and in many cases the nearest pixels are adopted. The estimation is depicted in Eq. (1),

$$y(\mathbf{s}_0) = \sum_{j=1}^{k} c_j y(\mathbf{s}_j), \tag{1}$$

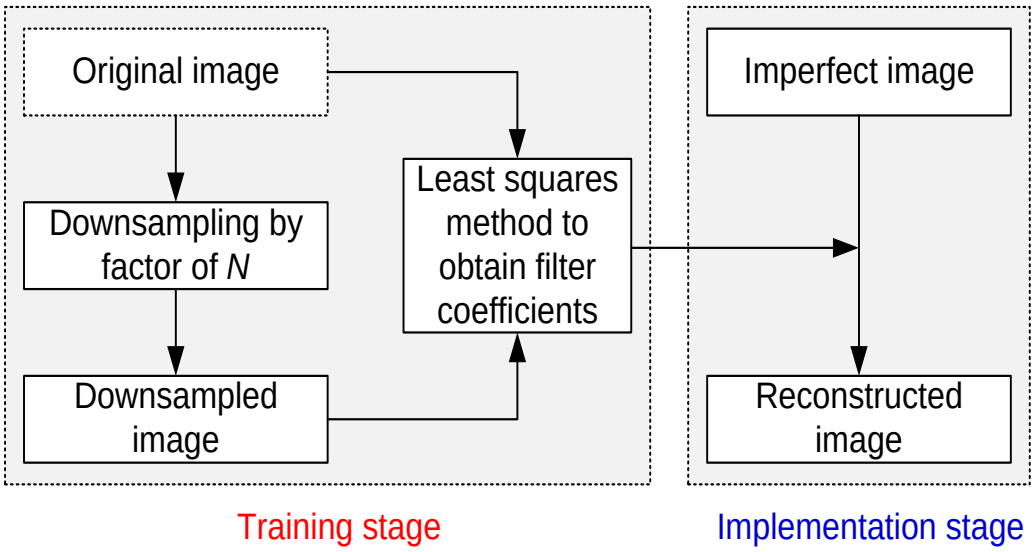

Figure 2. (a) An Example of Optical Image and (b) Thermal Infrared Image of (a) Obtained by FLIR Infrared Camera

The obtained coefficients for LSM estimation is locally optimized in a least-square sense. One of the useful selections of a training window is a rectangular-shape window which has $U=2p(p+1)$ elements, where p is the size of training window: $p+1$ is vertical direction size and p is horizontal direction size. Then, the training progression is organized in a U by 1 column vector $z=[y(s\text{-}1), y(s\text{-}2),\ldots, y(s\text{-}U)]$. By the estimation neighbors, one can form an $U\times V$ matrix

$$A = \begin{bmatrix} y(s-1-1) & y(s-1-2) & \ldots & y(s-1-V) \\ y(s-2-1) & y(s-2-2) & \ldots & y(s-2-V) \\ \ldots & \ldots & \ldots & \ldots \\ y(s-U-1) & y(s-U-2) & \ldots & y(s-U-V) \end{bmatrix}, \tag{2}$$

Now, the optimal coefficients can be obtained by traditional least squares method.

$$\mathbf{c} = (A^T A)^{-1}(A^T z) \tag{3}$$

which is the solution of

$$\hat{\mathbf{c}} = \arg\min_{\mathbf{c}} \left(\|\mathbf{z} - \mathbf{A}\mathbf{c}\|_2 \right), \tag{4}$$

3. Simulation Results

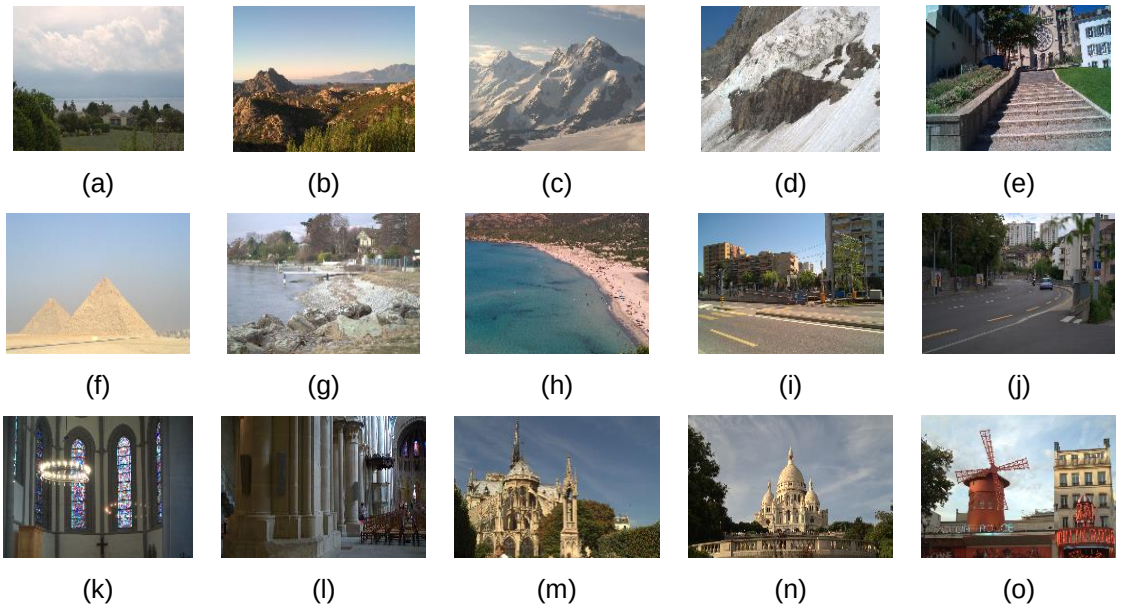

Figure 3. 15 Original Test Images for Comparison. Labels (a) to (o) are #1 to #15

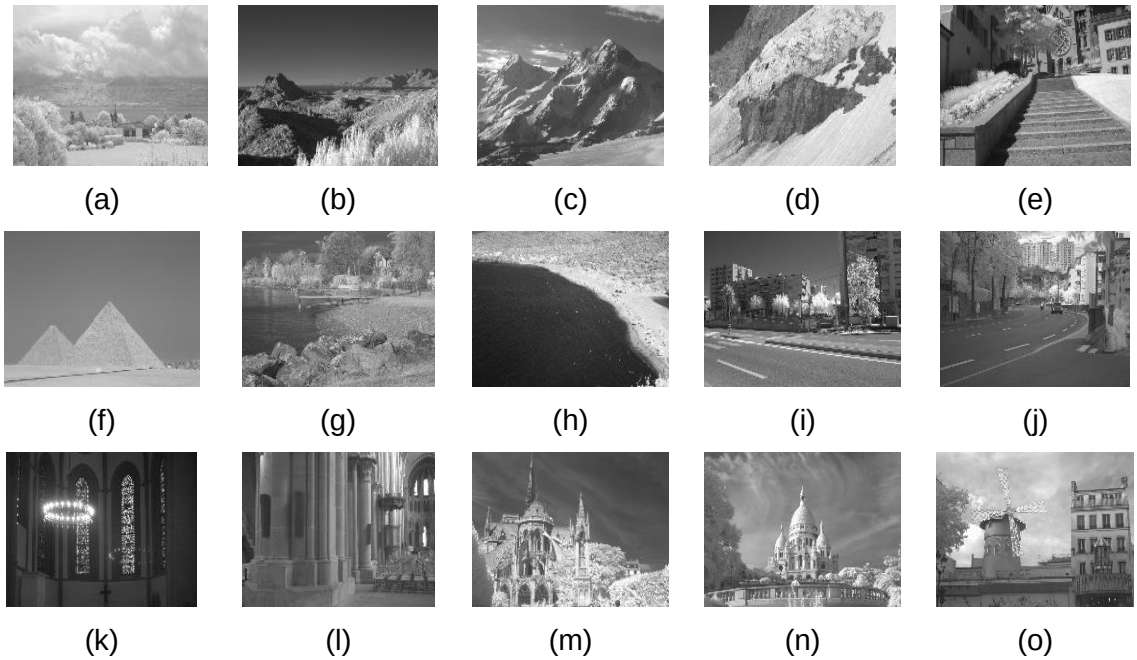

Figure 4. 15 Infrared Test Images for Comparison. Labels (a) to (o) are #1 to #15

To assess the efficiency of the proposed filters, we compared our filters with ground truth (bilinear method). The test images include 15 RGB images shown in Figure 3 and its thermal images (NIR: near-infrared) are shown in Figure 4. The scene dataset we used is accessible

[13]. The imageset comprise of 477 test images in nine different classes saved in RGB and NIR. The nine classes include country, field, forest, indoor, mountain, oldbuilding, street, urban, and water categories. For more information of the imageset, one may download images. The parameter *N* is assigned as 2.

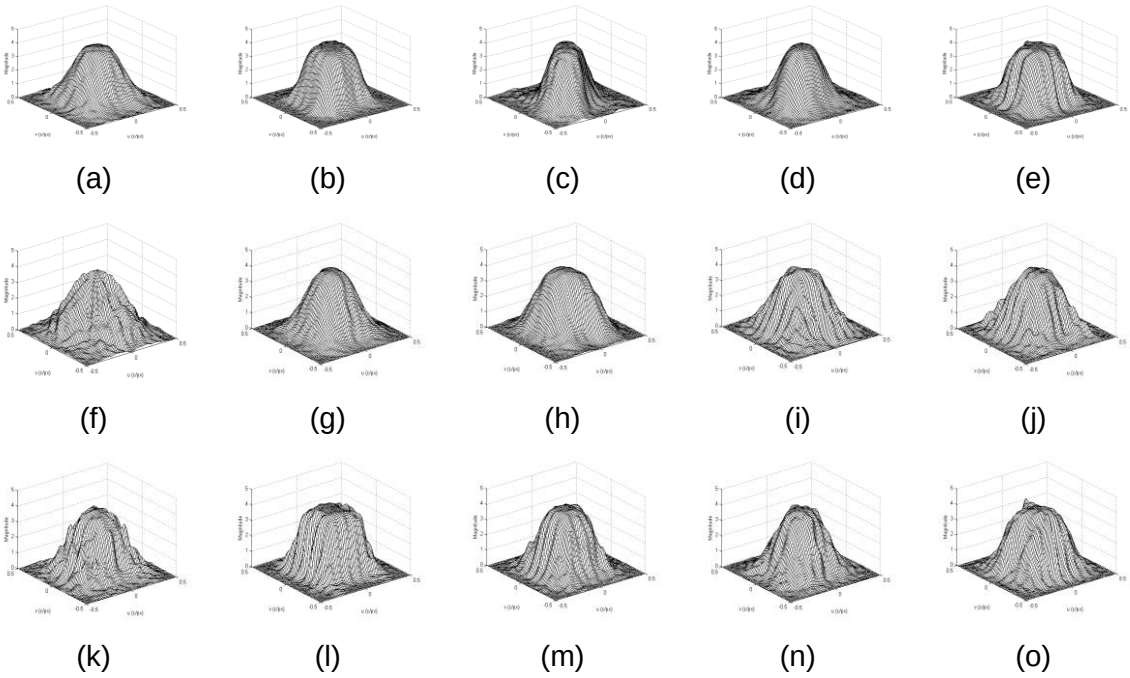

Figure 5. Designed 23×23 Filters for Each Test Infrared Image. Labels (a) to (o) are #1 to #15

Figure 5 shows the frequency response of 15 filters obtained by 15 different images. Depend on the training image, the shape of the frequency response is varying. From frequency response, it is clearly seen that image #4 has less high-frequency energy in a test image, while image #6 has more high-frequency energy in a test image. Note that the low frequency energy gathers at [0,0] position on the power spectrum density, and high frequency energy is displayed at the left-right (horizontal direction), up-down (vertical direction), or corner side (diagonal direction) of the power spectrum density.

Figure 6 shows the reconstructed images using image #14. Figure 6(a) is obtained using bilinear method and Figure 6(b) is obtained using the proposed 23×23 size filter. Figures 6(c) and 6(d) are difference images between original images and the reconstructed ones. Since the color of the images are inverted from 0 to 255 and 255 to 0, less intensity implies less artifacts on the reconstructed images. In other words, Figure 6(c) shows more values with less intensity, Figure 6(c) is visually better results. In the same manner, Figure 7 can be interpreted as above (Figure 6).

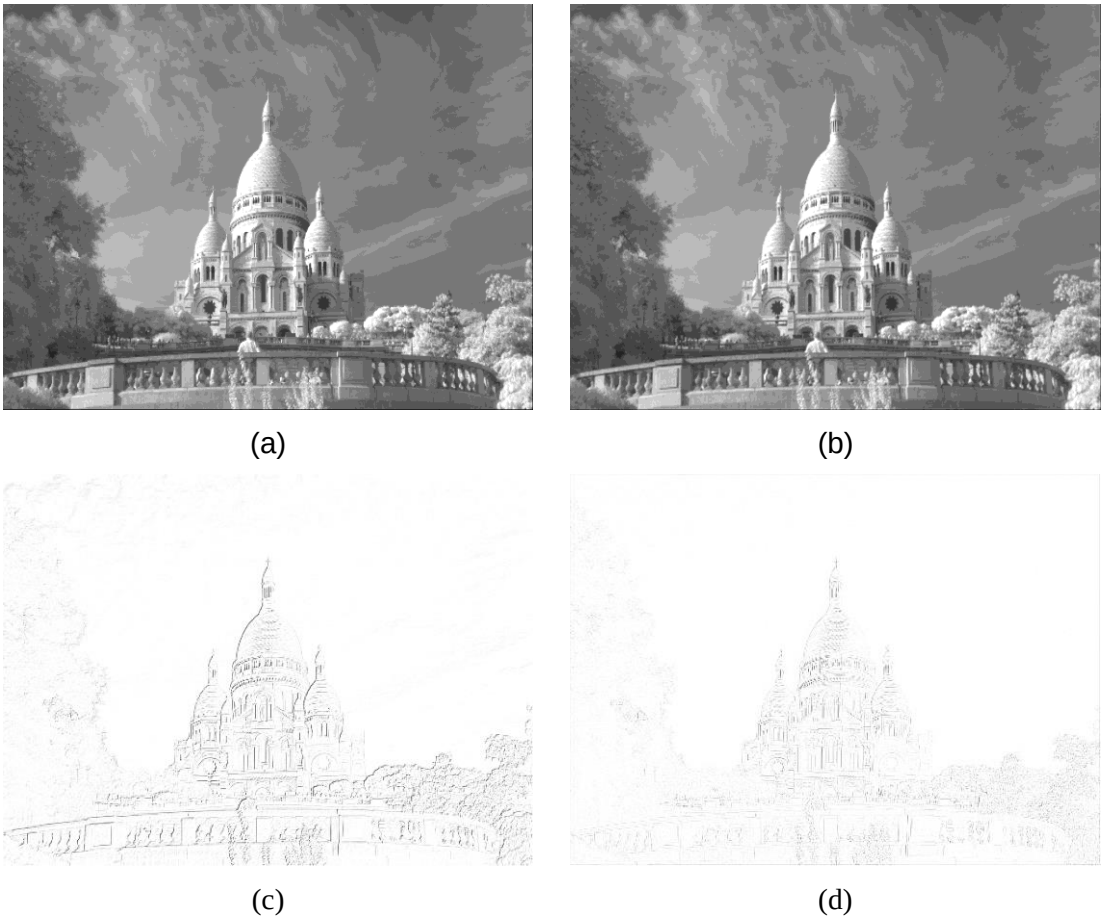

Figure 6. Visual Performance Comparison using #14 Image: (a) Reconstructed #14 Image with Bilinear Method, (b) Reconstructed #14 Image with Designed 23×23 Size Filter, (c) Image Difference between Original Image and the Bilinear Method used One, (d) Image Difference between Original Image and the Designed 23×23 Size Filter Used one. Note that (c) and (d) are Color Inverted Results

Figure 8 shows the performance between bilinear method and the proposed filter with 3×3 size. As we can see the proposed filter shows 3.5 dB better peak signal-to-noise ratio (PSNR) on 15 test images. Figures 9 and 10 show the PSNR difference comparison between different sized filters: 3×3, 5×5, 7×7, 9×9, 11×11, 13×13, 15×15, 17×17, 19×19, 21×21, and 23×23. We assume 3×3 filter is the ground truth, thus if PSNR result is positive numbers, bigger filter gives better performance. Interestingly, it is found from Figs. 9 and 10 that bigger filter does not always give better results (image #6). As can be seen from Figures 9 and 10, as filter size growing, the PSNR results goes down -0.2 dB.

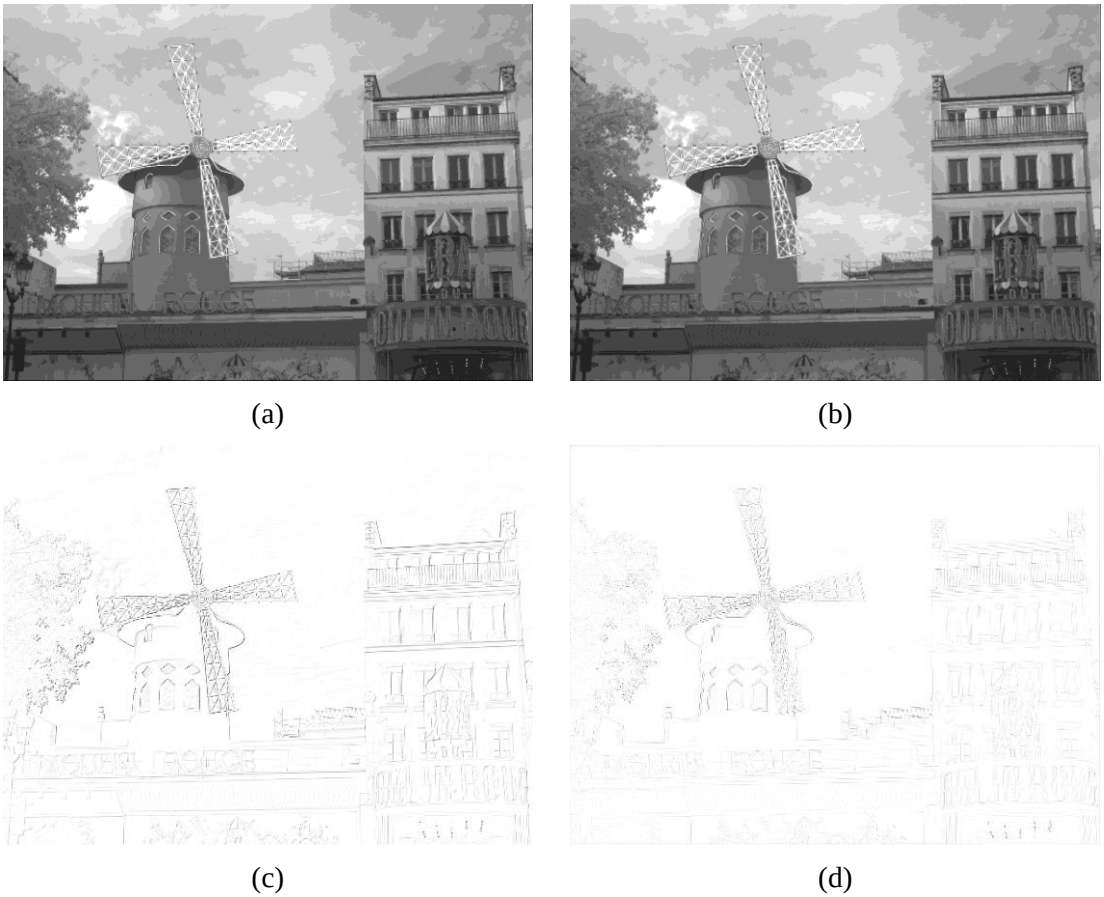

(a) (b)

(c) (d)

Figure 7. Visual Performance Comparison using #15 Image: (a) Reconstructed #15 Image with Bilinear Method, (b) Reconstructed #15 Image with Designed 23×23 Size Filter, (c) Image Difference between Original Image and the Bilinear Method used One, (d) Image Difference Between Original Image and the Designed 23×23 Size Filter used One. Note that (c) and (d) are Color Inverted Results

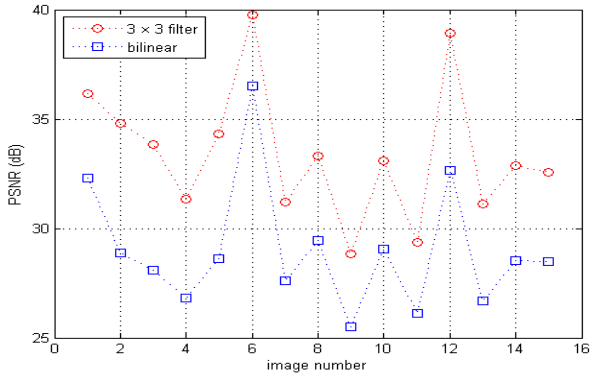

Figure 8. PSNR Performance Comparison between Bilinear Method and the Proposed 3×3 size Filter

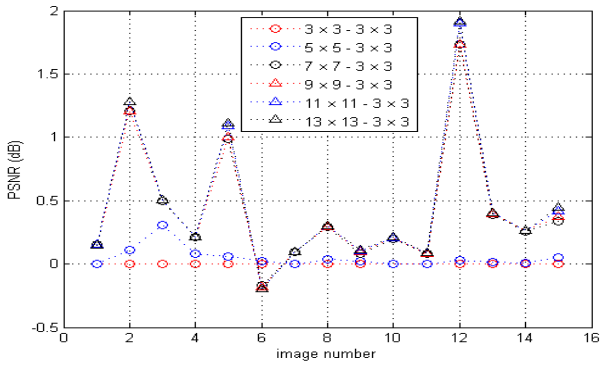

Figure 9. PSNR Difference Comparison between Different Sized Filters: 3×3, 5×5, 7×7, 9×9, 11×11, and 13×13. The 3×3 Filter is the Ground Truth

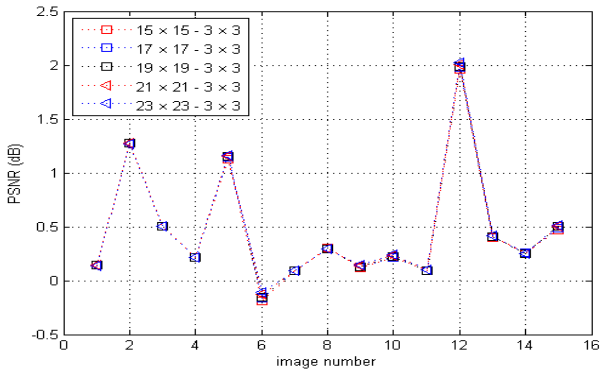

Figure 10. PSNR Difference Comparison between Different Sized Filters: 15×15, 17×17, 19×19, 21×21, and 23×23. The 3×3 Filter is the Ground Truth

4. Conclusions

In this paper, a new thermal infrared images upsampling method was introduced. As the resolution of thermal infrared images is smaller than that of color image obtained by digital camera via CFA, image upsampling method is necessary. To meet this request, filter design approach in training stage was proposed. The implementation stage proves our method is feasible. Simulation results show the PSNR performance in detail.

Acknowledgements

This research was supported by Basic Science Research Program through the National Research Foundation of Korea(NRF) funded by the Ministry of Science, ICT and Future Planning(2013R1A1A1010797).

References

[1] Available: http://www.flir.com/.
[2] A. Pretto, E. Menegatti, P. Bison, E. Grinzato, G. Cadelano and E. Pagello, “An autonomous robotized system for a thermographic camera”, Proc. IEEE 6th German Conference on Robotics (ROBOTIK), **(2010)**, pp. 1-8.

[3] C. F. Gottlieb, M. J. Hagmann, T. M. Babij, A. Markoe, J. G. Schwade and P. V. Houdek, "Heating patterns of interstitial and external microwave hyperthermia applicators determined using a miniature electric field probe, thermographic camera, and point temperature measurements", Proc. Annual International Conference of the IEEE, Engineering in medicine and biology society, **(1991)**, pp. 968-969.
[4] A. Pavlovic, Z. Barbaric and V. Nikolic, "Analysis of thermal images in thermography studio software package", Proc. 19th Telecommunications Forum (TELFOR), **(2011)**, pp. 627-630.
[5] A. M. Guzman, M. Goryawala and M. Adjouadi, "Generating thermal facial signatures using thermal infrared images", Proc. IEEE Emerging Signal Processing Applications (ESPA), **(2012)**, pp. 21-24.
[6] Z. Wang and S. Wang, "Spontaneous facial expression recognition by using feature-level fusion of visible and thermal infrared images", Proc. IEEE Machine Learning for Signal Processing (MLSP), **(2011)**, pp. 1-6.
[7] Q. Guo, C. Yang and C. Wei, "A new approach to the on-orbit evaluation of point spread function of thermal infrared images with applications to FY-2 satellite products", IEEE Trans. Geoscience and Remote Sensing, vol. 48, no. 3, **(2010)**, pp. 1598-1612.
[8] W. T. Gustafson and A. Gillespie, "Onboard processing of orbital hyperspectral thermal infrared images", Proc. IEEE Aerospace Conference Proceedings, vol. 5, **(2002)**, pp. 206-2070.
[9] I. Danilina, A. Gillespie, L. Balick, A. Mushkin, M. Smith and M. O'Neal, "Subpixel roughness effects in spectral thermal infrared emissivity images", Proc. IEEE Hyperspectral Image and Signal Processing: Evolution in Remote Sensing, **(2009)**, pp. 1-4.
[10] A. Tangherlini, A. Merla, and G.L. Roman, "Field-warp registration for biomedical high-resolution thermal infrared images," in Proc. Engineering in Medicine and Biology Society, 2006, pp. 961-964.
[11] J. Konopacki and K. Moscinska, "A simplified method for IIR filter design with quasi-equiripple passband and least-squares stopband," in Proc. IEEE Electronics, Circuits and Systems, 2007, pp. 302-305.
[12] C.-L. Fan and M.-Y. Pang, "A method for filtering noise data by blending local least squares fitting curves", in Proc. IEEE Computer Science and Engineering, **(2009)**, pp. 538-542.
[13] Available: http://ivrg.epfl.ch/supplementary_material/cvpr11/.

Author

Gwanggil Jeon received the BS, MS, and PhD (summa cum laude) degrees in Department of Electronics and Computer Engineering from Hanyang University, Seoul, Korea, in 2003, 2005, and 2008, respectively.

From 2008 to 2009, he was with the Department of Electronics and Computer Engineering, Hanyang University, from 2009 to 2011, he was with the School of Information Technology and Engineering (SITE), University of Ottawa, as a postdoctoral fellow, and from 2011 to 2012, he was with the Graduate School of Science & Technology, Niigata University, as an assistant professor. He is currently an assistant professor with the Department of Embedded Systems Engineering, Incheon National University, Incheon, Korea. His research interests fall under the umbrella of image processing, particularly image compression, motion estimation, demosaicking, and image enhancement as well as computational intelligence such as fuzzy and rough sets theories.

He was the recipient of the IEEE Chester Sall Award in 2007 and the 2008 ETRI Journal Paper Award.